A New MIMO ORC Architecture for Power Oscillation Damping using Remote Feedback Signals under Intermittent Observations

Amirthagunaraj Yogarathinam, *Student Member, IEEE*, and Nilanjan Ray Chaudhuri, *Senior Member, IEEE*

***Abstract*—A new multi-input multi-output (MIMO) Observer-driven Reduced Copy (ORC) i.e. MIMO-ORC architecture is proposed for wide-area damping control using multiple doubly fed induction generator-based wind farms to mitigate the issue of intermittent observations with multiple feedback signals and actuators. In this context, the concepts of cyber-physical self-coupling and cross-coupling are introduced and their impact on deterioration of closed-loop performance with data dropout is quantified through an analytical derivation. A framework for stability analysis of MIMO-ORC architecture is also proposed. Finally, time-domain simulations show superiority of the proposed approach over its single-input single-output (SISO) ORC counterpart in a 16-machine New England-New York power system.**

***Index Terms*—DFIG, MIMO-ORC, PMU, Wide-Area Power Oscillation Damping, Data-dropout, Wind Farm.**

NOMENCLATURE

$i_{rdq-mod}$	DFIG RSC current modulation signals
x_{rr1}, x_{rr2}	DFIG RSC current controller states
x_{g1}, x_{g2}	DFIG GSC current controller states
G_n	reduced-order model of nominal (n) system
C_{n1}, C_{n2}	rows of the matrix C_n
B_{n1}, B_{n2}	columns of the matrix B_n
G_{on}	reduced-order model of off-nominal (on) system
C_{on1}, C_{on2}	rows of the matrix C_{on}
B_{on1}, B_{on2}	columns of the matrix B_{on}
K	state feedback gain matrix for MIMO-ORC
K_i	i^{th} row of K
L_i	observer gain vector for i^{th}-loop MIMO-ORC
$\hat{K}_1/\hat{K}_2$	state feedback gain vectors for SISO-ORC
$\hat{L}_i$	observer gain vector for i^{th}-loop SISO-ORC
x_{obi}	state vector estimated by i^{th}-loop observer
x_{ni}	state vector estimated by i^{th}-loop reduced copy
$\bar{x}_{obi}$	state vector received by i^{th}-loop receiver
x_{on}	state vector of the reduced power system under off-nominal condition
$u_i/\tilde{u}_i$	control input to i^{th}-loop reduced copy and observer/i^{th} actuator
y_{mi}	feedback signal from i^{th} PMU location
$\mathbf{\Psi_k}$	binary diagonal random matrix
A_{Cl}	state matrix of overall system dynamics during the time interval $t \in [t_k, t_{k+1})$
$\xi_i(t)/\xi_i'(t)$	error between the reduced-order power system state trajectory and that of reduced copy for i^{th}-loop of MIMO-ORC/SISO-ORC
R/μ	data receiving rate as % / p.u.
$A_d(q)$	state matrices of Jump Linear System
$\rho(M)$	spectral radius of matrix M
W	state transition probability matrix of Markov chain governing system's mode switches
$\boldsymbol{P}\{X\}$	probability of event X
$\|\cdot\|$	Euclidian norm of a vector or a matrix
$\times/\otimes$	matrix multiplication/Kronecker product
$\mathcal{L}$	Laplace operator
Υ	sampling period of communication channel
Π_0	initial state probability distribution of Markov chain governing system's mode switches
ORC	Observer-driven Reduced Copy
NCS	Networked Control Systems
CPS	Cyber-Physical System
DFIG	Doubly-Fed Induction Generator
POD	Power Oscillation Damper
RSC	Rotor-Side Converter
JLS	Jump Linear System
PSS	Power System Stabilizer
LQR	Linear Quadratic Regulator

The authors are with the School of Electrical Engineering & Computer Science, The Pennsylvania State University, University Park, PA 16802, USA (e-mail: *axy43@psu.edu, nuc88@psu.edu*).

Financial support from NSF under grant award CNS 1657024 is gratefully acknowledged.

I. INTRODUCTION

In recent years, several power system researchers [1]–[5] studied Doubly Fed Induction Generator (DFIG)-based wind farms installed with power oscillation damper (POD) for Wide-Area Damping Control (WADC). However, utilities with years of experience in PMU proliferation are contemplating a wider use of networked communication to utilize the available bandwidth, partly for WADC usage, and partly for providing other data intensive services like video-conference facility [6]–[10], which brings challenges like latency and packet drop. Most of the researchers [3]–[5] on the WADC using wind farms have not adequately considered the packet drop issue while latency in the cyber layer was taken into account.

In contrast, networked control system (NCS) literature on model-based control [11]–[14] has studied the issue of packet drop. However, it appears that [11]–[14], have traditionally used the single-input single-output (SISO) 'reduced copy' or SISO Observer-driven Reduced Copy (ORC) i.e. SISO-

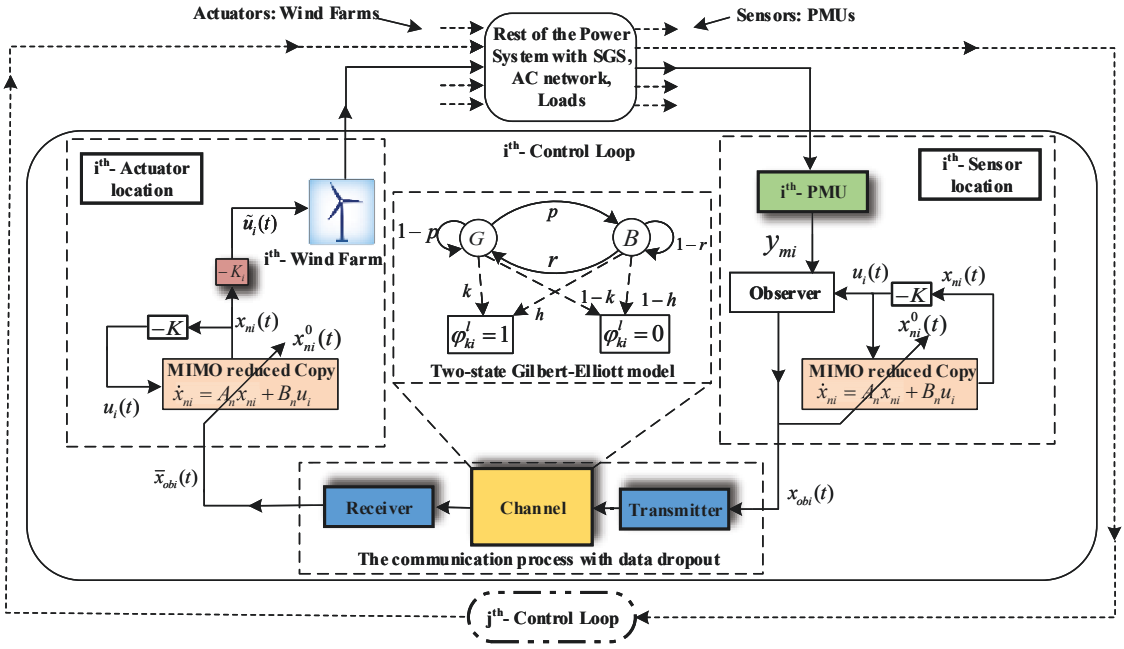

Fig. 1. Overall architecture of the proposed MIMO-ORC approach. The i^{th} control loop is shown in detail. It can be noted that for the i^{th} loop at the actuator location the i^{th} row of the controller gain matrix K is used. The two-state Gilbert-Elliott model is used to represent the stochastic data dropout in the communication link.

ORC architecture to overcome this issue. Apparently, there is no study on the multi-input multi-output (MIMO) 'reduced copy' or MIMO-ORC architecture. It can be hypothesized that, *when multiple feedback signals are used along with multiple actuators, a MIMO 'reduced copy' is likely to have a better representation of the system dynamics as compared to multiple SISO 'reduced copy.'*

Thus motivated, in this paper, for the first time, a new MIMO-ORC architecture is proposed in which each of the multiple actuators uses a MIMO 'reduced copy.' Moreover, in this paper, the concepts of cyber-physical 'self-coupling' and 'cross-coupling' are introduced in the context of MIMO- and SISO-ORC architectures. Then, the effect of these couplings on the deterioration of closed-loop performance is quantified using an analytical measure. Finally, a framework for stability analysis of the MIMO-ORC architecture is also presented. The proposed concepts are applied in a power grid to mitigate the problem of wide-area power oscillation damping control under data packet dropout. References [15] and [16] have considered this issue when a single actuator is used. In contrast, we will focus our attention on the scenario in which multiple inter-area modes are damped using multiple actuators and feedback signals in presence of data dropout.

In this context, our recent work [17] and [18] has taken into account multiple wind farms as actuators and multiple PMU signals for feedback. Inspired by the NCS literature on model-based control [11]–[15], references [17] and [18] used an ORC architecture where each actuator employs a SISO reduced-order model as the 'reduced copy.' In contrast to [15] and [17], [18], in this paper:

- a new MIMO-ORC architecture is proposed, which uses a MIMO 'reduced copy' at each actuator location.
- an analytical derivation is presented that takes into account the effect of data dropout in one link on the performance of the MIMO/SISO 'reduced copy,' which uses another link.
- a framework for stability analysis of MIMO-ORC architecture is proposed.
- effectiveness of the MIMO-ORC is compared with SISO-ORC using linear and nonlinear time-domain simulations for WADC in a power grid.

II. Proposed MIMO-ORC Architecture for Power Oscillation Damping

The overall architecture of the proposed MIMO-ORC approach is shown in Fig. 1. The ORC architecture presented in [17] utilizes a SISO reduced-order model as the 'reduced copy' for each control loop. In contrast, the MIMO-ORC approach proposed in this paper utilizes MIMO reduced-order model as the 'reduced copy' for each control loop, see Fig. 1.

A. Study System

The effectiveness of the proposed MIMO-ORC architecture is tested using a 16-machine, 5-area dynamic equivalent of the New England-New York system, see Fig. 2.

A nonlinear positive sequence fundamental frequency phasor model is considered. All the synchronous generators (SGs) are represented by sixth-order subtransient models and eight of them (G1-G8) are equipped with the IEEE type DC1A excitation system. SG G9 is equipped with a static exciter and a power system stabilizer (PSS). The dynamic data of the power system and the nominal power transfer through tie lines can be found in [19].

In this study, two SGs (G9 and G15) are replaced with two

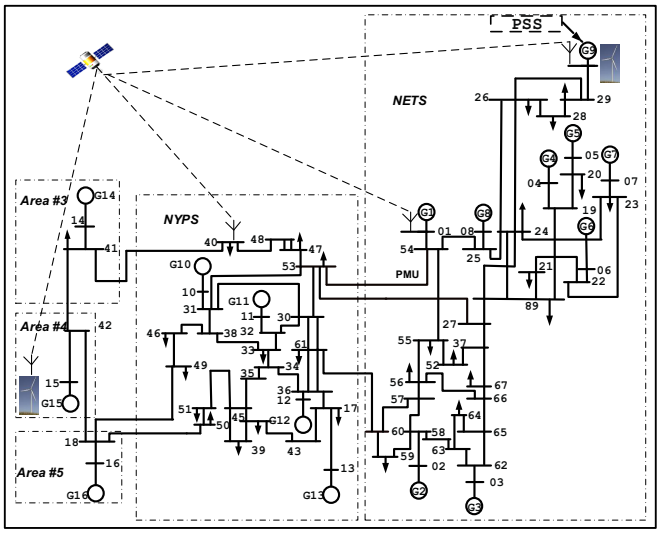

Fig. 2. 16-machine, 5-area equivalent representing New England - New York power system. Wind farms are connected to bus-9 and bus-15.

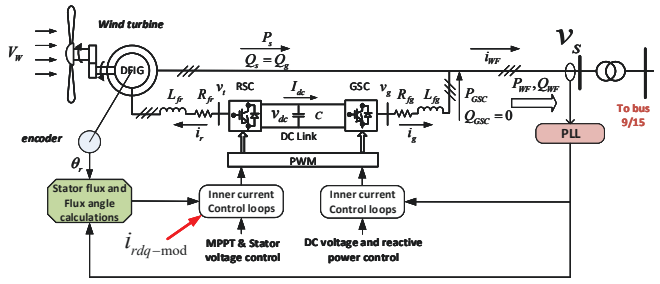

Fig. 3. Schematic of DFIG-based wind turbine with its overall control architecture. The modulation signals i_{rd-mod} or i_{rq-mod} are used to damp the inter-area oscillation.

equivalent DFIG-based wind farms. The schematic of the DFIG-based wind farms with its overal control architecture is shown in Fig. 3, which is represented by an aggregated model whose turbine-generator rotational dynamics is represented by a two-mass model to include the torsional mode. The generator is modeled using standard differential and algebraic equations as given in [20]. The turbine is assumed to operate in the zone of maximum power point extraction. Also, the blade pitch angle and the wind speed is assumed to be constant. The tie-reactors of the VSCs, DC-link dynamics and the PLL dynamics are included in the model. In the standard notation, the state-variables x of the DFIG-based wind farm model are:

$$x = [i_{qs} \quad i_{ds} \quad e'_{qs} \quad e'_{ds} \quad i_{qg} \quad i_{dg} \quad i_{ms} \quad \omega_{r\_dfg} \quad \omega_t \quad \theta_{tw} \quad v_{dc}^2 \quad x_{rr1} \quad x_{rr2} \quad x_{g1} \quad x_{g2} \quad \hat{\theta}_2 \quad x_{pll(2)} \quad i^*_{qg} \quad x_v]^T \tag{1}$$

Here, $\hat{\theta}_2$ and $x_{pll(2)}$ are the PLL states, and i^*_{qg} and x_v are the state-variables of the DC-link voltage controller. For more details of DFIG model and controls used in this paper, the readers are referred to [20], [21]. In this study, for each wind farm either of the modulation signals i_{rd-mod} or i_{rq-mod} are used to damp the inter-area oscillation, see Fig. 3.

B. Proposed MIMO-ORC Approach

The linearized power system model around the nominal operating point is reduced to the lowest possible order (in this study a $15^{th}-$order model) such that the MIMO reduced-order system (G_n) reasonably represents the dynamics of the full-order system in the frequency range of electromechanical modes. This reduced-order model is described by:

$$G_n = \left[\begin{array}{c|c} A_n & B_n \\ \hline C_n & 0 \end{array}\right] \tag{2}$$

For simplicity, we restrict our case to two wind farms working as actuators.

In this case, the reduced-order system G_n is a 2-input - 2-output system. Therefore, B_n and C_n can be decomposed as:

$$B_n = \left[\begin{array}{cc} B_{n1} & B_{n2} \end{array}\right], \qquad {C_n}^T = \left[\begin{array}{cc} {C_{n1}}^T & {C_{n2}}^T \end{array}\right] \tag{3}$$

As shown in Fig. 1, an observer at the sensor location uses a multi-input single-output (MISO) reduced-order linearized model G_n of the system to estimate the states $x_{obi}(t)$ given by:

$$\begin{aligned} \dot{x}_{obi}(t) &= A_n x_{obi}(t) + B_n u_i(t) + L_i(y_{mi}(t) - \bar{y}_{mi}(t)) \\ \bar{y}_{mi}(t) &= C_{ni} x_{obi}(t), \qquad for \quad i = 1,\ 2 \end{aligned} \tag{4}$$

It is important to note here that the observer uses only one feedback signal (y_{m1} or y_{m2}) and the corresponding row of the C matrix (C_{n1} or C_{n2}). For the i^{th} control loop, estimates of the dynamic states $x_{obi}(t)$ are sent over the communication network to the wind farms. Control input signals $u_i(t)$ at the actuator locations and the sensor locations are calculated using MIMO 'reduced copy' of the system at each place (see Fig. 1). For each control loop the 'reduced copy' dynamics and the control input signals $u_i(t)$ are described by:

$$\dot{x}_{ni}(t) = A_n x_{ni}(t) + B_n u_i(t), \qquad for \quad i = 1,\ 2 \tag{5}$$

$$u_i(t) = -K x_{ni}(t), \qquad for \quad i = 1,\ 2 \tag{6}$$

where K is the state-feedback controller gain vector, which can be decomposed as follows:

$$K^T = \left[\begin{array}{cc} K_1^T & K_2^T \end{array}\right] \tag{7}$$

When a new data-packet is available, it is used to reset the dynamic states of the 'reduced copy' in both sending and receiving ends at the same instant. Let the 'reduced copy' at both locations be reset with the sample x^0_{nik} at time sample t_k satisfying:

$$x^0_{nik} = \mathbf{\Psi_{ik}} x_{obik} + (I - \mathbf{\Psi_{ik}}) x_{nik}, \qquad for \quad i = 1,\ 2 \tag{8}$$

where, x_{nik} are the dynamic states estimated by the i^{th} 'reduced copy' when new data packets do not arrive. Data dropout in the communication channels are represented by two independent random variables $\mathbf{\Psi_{1k}}$ and $\mathbf{\Psi_{2k}}$. When data drops out and fails to reach the wind farm, the states of both the 'reduced copy' are allowed to evolve naturally. Otherwise, the proposed architecture resets the states of both 'reduced copy' in a control loop.

In this paper, the transmitter and the receiver, see Fig. 1, are

represented by zero-order-hold (ZOH) and sample and hold (S/H) circuits, respectively. The stochastic data dropout is represented by the two-states (Good (G), Bad (B)) Gilbert-Elliott model, see Fig. 1, where both states produce errors with different probabilities. For more information regarding the Gilbert-Elliott model, readers are referred to [17].

The variable $\mathbf{\Psi_{ki}} = diag(\varphi^1_{ki}, \varphi^2_{ki}, ..., \varphi^n_{ki})$ is a binary diagonal random matrix and each φ^l_{ki} follows a stochastic random variation with the understanding that $\varphi^l_{ki} = 1$ (having a probability of $(1 - P_E)$) signifies that the l^{th} element of the vector x_{obik} reaches its destination and that $\varphi^l_{ki} = 0$ (having a probability of P_E) when it does not. In this study, $\varphi^l_{ki} = \varphi^j_{ki}$ for $l \neq j$ is assumed since all the elements of the vector x_{obik} is part of the same data packet.

In the following section, the concepts of cyber-physical 'self-coupling' and 'cross-coupling' are introduced.

III. Concepts of Cyber-Physical Self-Coupling and Cross-Coupling

Cyber-Physical 'Self-Coupling': We define this as the interaction between the communication channel used for i^{th} feedback signal with the physical plant, which influences the closed-loop performance of the i^{th} loop. For example data-dropout in the i^{th} communication channel will affect the performance of the i^{th} loop, see Fig. 1.

Cyber-Physical 'Cross-Coupling': We define this as the interaction between the communication channel used for a *different* feedback signal (e.g., in the j^{th} loop) with the physical plant, which influences the closed-loop performance of the i^{th} loop, see Fig. 1.

Next, we will quantify the impact of these coupling mechanisms on the closed-loop performance of MIMO- and SISO-ORC architectures using analytical measures. For simplicity, we restrict our case to two wind farms working as actuators.

Cyber-Physical Coupling in MIMO-ORC Architecture:
Let us consider the reduced-order state-space model of the power system under off-nominal operating condition (e.g. higher loading), which is given by:

$$\begin{aligned}\dot{x}_{on}(t) &= A_{on}x_{on}(t) + B_{on}\tilde{u}\,(t)\\ &= A_{on}x_{on}(t) + \begin{bmatrix} B_{on1} & B_{on2}\end{bmatrix}\begin{bmatrix}\tilde{u}_1\,(t)\\ \tilde{u}_2\,(t)\end{bmatrix}\\ y_m(t) &= \begin{bmatrix} y_{m1}(t)\\ y_{m2}(t)\end{bmatrix} = C_{on}x_{on}(t) = \begin{bmatrix} C_{on1}\\ C_{on2}\end{bmatrix}x_{on}(t)\end{aligned} \tag{9}$$

where the subscript 'on' denotes the off-nominal system. The control input to the plant $(\tilde{u})$, see Fig. 1, is given by:

$$\tilde{u} = \begin{bmatrix}\tilde{u}_1\\ \tilde{u}_2\end{bmatrix} = \begin{bmatrix} -K_1x_{n1}\\ -K_2x_{n2}\end{bmatrix} \tag{10}$$

where, x_{n1} and x_{n2} are the dynamic states estimated by the 'reduced copy' at the actuator locations as given in equation (5). Combining equations (4), (5), the reduced-order power system dynamics under off-nominal condition from (9), and the control input to the plant from (10); one can derive the overall system dynamics during the time interval $t \in [t_k, t_{k+1})$, $t_{k+1} - t_k = \Upsilon$ as:

$$\begin{pmatrix}\dot{x}_{on}\\ \dot{x}_{n1}\\ \dot{x}_{n2}\\ \dot{x}_{ob1}\\ \dot{x}_{ob2}\end{pmatrix} = A_{Cl}\begin{pmatrix} x_{on}\\ x_{n1}\\ x_{n2}\\ x_{ob1}\\ x_{ob2}\end{pmatrix} \tag{11}$$

where,

$$A_{Cl} = \begin{bmatrix} A_{on} & -B_{on1}K_1 & -B_{on2}K_2 & \mathbf{0} & \mathbf{0}\\ \mathbf{0} & a_{22} & \mathbf{0} & \mathbf{0} & \mathbf{0}\\ \mathbf{0} & \mathbf{0} & a_{33} & \mathbf{0} & \mathbf{0}\\ L_1C_{on1} & -B_nK & \mathbf{0} & a_{44} & \mathbf{0}\\ L_2C_{on2} & \mathbf{0} & -B_nK & \mathbf{0} & a_{55}\end{bmatrix}$$

$$\begin{aligned} &a_{22} = a_{33} = A_n - B_nK, \qquad a_{44} = A_n - L_1C_{n1}\\ &a_{55} = A_n - L_2C_{n2}\end{aligned} \tag{12}$$

Accuracy of the estimated states by the 'reduced copy' would be affected when the system is under off-nominal conditions and communication channels have low data receiving rates (R). Therefore, it would be useful to estimate the state trajectories of the reduced copies during the inter-sample interval.

From the dynamics of the combined nominal, off-nominal and observer systems (11) during the inter-sample period $[t_k, t_{k+1})$, it is observed that the responses of $x_{on}(t)$, $x_{n1}(t)$, and $x_{n2}(t)$ are uncoupled with that of the observer states $x_{ob1}(t)$ and $x_{ob2}(t)$. Hence, the left upper block can be considered separately for analysis during $t \in [t_k, t_{k+1})$. Thus, neglecting the observer dynamics without loss of generality, (11) can be rewritten as:

$$\begin{pmatrix}\dot{x}_{on}\\ \dot{x}_{n1}\\ \dot{x}_{n2}\end{pmatrix} = \begin{bmatrix} A_{on} & -B_{on1}K_1 & -B_{on2}K_2\\ \mathbf{0} & A_n - B_nK & \mathbf{0}\\ \mathbf{0} & \mathbf{0} & A_n - B_nK\end{bmatrix}\begin{pmatrix} x_{on}\\ x_{n1}\\ x_{n2}\end{pmatrix} \tag{13}$$

Let,

$$\Omega = \begin{bmatrix} A_{on} & -B_{on1}K_1 & -B_{on2}K_2\\ \mathbf{0} & A_n - B_nK & \mathbf{0}\\ \mathbf{0} & \mathbf{0} & A_n - B_nK\end{bmatrix} \tag{14}$$

and the initial condition be:

$$\begin{bmatrix} x_{on}\,(t_k) & x_{n1}\,(t_k) & x_{n1}\,(t_k)\end{bmatrix}^T = \begin{bmatrix} x^0_{onk} & x^0_{n1k} & x^0_{n2k}\end{bmatrix}^T \tag{15}$$

Solution of (13) for $t \in [t_k, t_{k+1})$ is given by:

$$\begin{pmatrix} x_{on}(t)\\ x_{n1}(t)\\ x_{n2}(t)\end{pmatrix} = e^{\Omega(t-t_k)}\begin{pmatrix} x^0_{onk}\\ x^0_{n1k}\\ x^0_{n2k}\end{pmatrix} \tag{16}$$

Equation (16) represents the temporal evolution of the system states of the reduced-order model and those of the reduced copy. The state trajectory of reduced copies with initial states $(x^0_{nik}\ for\ \ i = 1\ or\ 2)$ can be expressed for $t \in [t_k, t_{k+1})$ as:

$$x_{ni}(t) = e^{(A_n - B_nK)(t-t_k)}(\mathbf{\Psi_{ik}}x_{obi} + (I - \mathbf{\Psi_{ik}})x_{nik}) \tag{17}$$

To find the expression for the state trajectory of the reduced-order linearized power system, equation (16) can be trans-

formed into the Laplace domain as follows:

$$\begin{pmatrix} X_{on}(s) \\ X_{n1}(s) \\ X_{n2}(s) \end{pmatrix} = \Lambda \begin{pmatrix} x^0_{onk} \\ x^0_{n1k} \\ x^0_{n2k} \end{pmatrix} \tag{18}$$

where:

$$\Lambda = \mathcal{L}\left\{e^{\Omega(t-t_k)}\right\} = (sI - \Omega)^{-1} \tag{19}$$

Using the Lemma (9.1.3) of [22] one can show that:

$$(sI-\Omega)^{-1} = \begin{bmatrix} (sI - A_{on})^{-1} & \Delta_1 & \Delta_2 \\ \mathbf{0} & \Xi & \mathbf{0} \\ \mathbf{0} & \mathbf{0} & \Xi \end{bmatrix} \tag{20}$$

where

$$\begin{aligned} \Delta_1 &= -(sI - A_{on})^{-1} B_{on1} K_1 (sI - (A_n - B_n K))^{-1} \\ \Delta_2 &= -(sI - A_{on})^{-1} B_{on2} K_2 (sI - (A_n - B_n K))^{-1} \\ \Xi &= (sI - (A_n - B_n K))^{-1} \end{aligned} \tag{21}$$

The detailed derivation for arriving at (20) from (19) is given in Appendix.

From (18) and (20), $X_{on}(s)$ can be written as:

$$X_{on}(s) = (sI - A_{on})^{-1} x^0_{onk} + \Delta_1\, x^0_{n1k} + \Delta_2\, x^0_{n2k} \tag{22}$$

Using (22) and (5) one can derive the system states as:

$$\begin{aligned} x_{on}(t) &= x_{n1}(t) + e^{A_{on}(t-t_k)}(x^0_{onk} - x^0_{n1k}) \\ &+ \int_{t_k}^{t} e^{A_{on}(t-\tau)} (\delta A - \delta(BK)_1) e^{(A_n - B_n K)\tau} x^0_{n1k} d\tau \\ &- \int_{t_k}^{t} e^{A_{on}(t-\tau)} B_{on2} K_2 e^{(A_n - B_n K)\tau} x^0_{n2k} d\tau \end{aligned} \tag{23}$$

where $\delta A = A_{on} - A_n$, $\delta(BK)_i = B_{oni}K_i - B_n K \quad for \quad i = 1,\ 2$ and $x_{ni}(t)$ are the reduced copies' states given by:

$$x_{ni}(t) = e^{(A_n - B_n K)(t-t_k)} x^0_{nik}, \qquad for \quad i = 1,\ 2 \tag{24}$$

As mentioned earlier, accuracy of the estimated states by the reduced copy would be affected when the system is under off-nominal conditions and/or communication channels have higher data dropout. The error between the reduced-order linearized system state trajectory and that of each reduced copies could be a measure of system performance, which can be defined as:

$$\xi_i(t) := x_{on}(t) - x_{ni}(t), \qquad for \quad i = 1\ ,\ 2 \tag{25}$$

From (23) and (24), $\xi_1(t)$ can be derived as:

$$\begin{aligned} \xi_1(t) &= e^{A_{on}(t-t_k)}(x^0_{onk} - x^0_{n1k}) \\ &+ \int_{t_k}^{t} e^{A_{on}(t-\tau)} (\delta A - \delta(BK)_1) e^{(A_n - B_n K)\tau} x^0_{n1k} d\tau \\ &- \int_{t_k}^{t} e^{A_{on}(t-\tau)} B_{on2} K_2 e^{(A_n - B_n K)\tau} x^0_{n2k} d\tau \end{aligned} \tag{26}$$

using (8) equation (26) can be written as:

$$\begin{aligned} \xi_1(t) &= e^{A_{on}(t-t_k)}(x^0_{onk} - x_{ob1}) \\ &+ e^{A_{on}(t-t_k)}(I - \mathbf{\Psi_{1k}}) \times (x_{ob1} - x_{n1k}) \\ &+ \int_{t_k}^{t} e^{A_{on}(t-\tau)} (\delta A - \delta(BK)_1) e^{(A_n - B_n K)\tau} \\ &\times (\mathbf{\Psi_{1k}}(x_{ob1} - x_{n1k}) + x_{n1k}) d\tau \\ &- \int_{t_k}^{t} e^{A_{on}(t-\tau)} B_{on2} K_2 e^{(A_n - B_n K)\tau} \\ &\times (\mathbf{\Psi_{2k}}(x_{ob2} - x_{n2k}) + x_{n2k}) d\tau \end{aligned} \tag{27}$$

Similarly, $\xi_2(t)$ can also be derived. This reveals the impact of the interaction between the cyber and the physical layer on the MIMO-ORC performance.

Remark I: It can be seen from (27) that the error is dependent on the cyber-physical 'self-coupling' determined by the first two terms. The last term indicates the impact of the cyber-physical 'cross-coupling.' Under nominal operation of MIMO-ORC:

$$\begin{aligned} &A_{on} = A_n \Rightarrow \delta(A) = \mathbf{0} \\ &B_{on} = B_n \Rightarrow \delta(BK)_1 = -B_{n2}K_2 \\ &x_{n1} = x_{n2} = x_n \end{aligned} \tag{28}$$

Assuming $x^0_{onk} = x_{ob1} = x_{ob2} = x_n$ i.e. that the observers track the actual states perfectly, it can be seen from equation (27) that $\xi_1(t) = 0$. In a similar manner it can be shown that $\xi_2(t) = 0$.

Cyber-Physical Coupling in SISO-ORC Architecture:

One can also derive a similar expression corresponding to (27) for SISO-ORC architecture with two actuators. Only the final expression is given here, which is:

$$\begin{aligned} \xi'_1(t) &= e^{A_{on}(t-t_k)}(x^0_{onk} - x'_{ob1}) \\ &+ e^{A_{on}(t-t_k)}(I - \mathbf{\Psi_{1k}}) \times (x'_{ob1} - x'_{n1k}) \\ &+ \int_{t_k}^{t} e^{A_{on}(t-\tau)} (\delta A - \tilde{B}_1 \hat{K}_1) e^{(A_n - B_{n1}\hat{K}_1)\tau} \\ &\times (\mathbf{\Psi_{1k}}(x'_{ob1} - x'_{n1k}) + x'_{n1k}) d\tau \\ &- \int_{t_k}^{t} e^{A_{on}(t-\tau)} B_{on2} \hat{K}_2 e^{(\bar{A}_{n2} - \bar{B}_{n2}\hat{K}_2)\tau} \\ &\times (\mathbf{\Psi_{2k}}(x'_{ob2} - x'_{n2k}) + x'_{n2k}) d\tau \end{aligned} \tag{29}$$

where, $\hat{K}_1$ and $\hat{K}_2$ are the controller gain vectors, $\tilde{B}_1 = B_{on1} - B_{n1}$, and $(A_n,\ B_{n1})$ and $(\bar{A}_{n2},\ \bar{B}_{n2})$ are the parameter associated with copy 1 and copy 2 of the SISO-ORC architecture. Note that the closed-loop system with the controller designed for Loop 1 (see Section V-B) is given by:

$$G_{cl1} = \left[\begin{array}{cc|c} A_{nF} & -B_{n1F}\hat{K}_1 & B_{n2F} \\ \hat{L}_1 C_{n1F} & A_n - B_{n1}\hat{K}_1 - \hat{L}_1 C_{n1} & \mathbf{0} \\ \hline C_{n2F} & \mathbf{0} & \mathbf{0} \end{array}\right] \tag{30}$$

where, 'F' denotes the full-order system and $\hat{L}_1$ is observer gain vector of copy 1. Matrices $\bar{A}_{n2}$ and $\bar{B}_{n2}$ are the state matrix and the input matrix of the reduced-model of G_{cl1}. Similarly, $\xi'_2(t)$ can also be derived.

Remark II: Equation (29) reveals the impact of cyber-physical 'self coupling' and 'cross-coupling' on the SISO-ORC performance. Under nominal operation of SISO-ORC, assuming the observers track the actual states perfectly, it can be shown

from equation (29) that $\xi_1'(t) \neq 0$. In a similar manner, it can also be shown that $\xi_2'(t) \neq 0$.
The above analysis demonstrates the advantage of the MIMO-ORC architecture over its SISO counterpart. The claims in Remark I and Remark II will be validated using linear time-domain simulations in Section VI-B.

IV. Stability Analysis Framework for MIMO-ORC

The focus of this section is to develop the stability analysis framework for the MIMO-ORC architecture proposed in this paper. Starting from (13), one can write the following in discrete domain:

$$\begin{pmatrix} x_{on}(k+1) \\ x_{n1}(k+1) \\ x_{n2}(k+1) \end{pmatrix} = e^{\Omega\Upsilon} \begin{pmatrix} x_{on}(k) \\ x_{n1}(k) \\ x_{n2}(k) \end{pmatrix} \tag{31}$$

As mentioned earlier, the proposed architecture resets the states of both 'reduced copy' in a control loop. Following (15) and (8), equation (31) can be written as:

$$\begin{pmatrix} x_{on}(k+1) \\ x_{n1}(k+1) \\ x_{n2}(k+1) \end{pmatrix} = e^{\Omega\Upsilon} \begin{pmatrix} x_{on}(k) \\ \mathbf{\Psi_{1k}} x_{ob1}(k) + (I - \mathbf{\Psi_{1k}}) x_{n1}(k) \\ \mathbf{\Psi_{2k}} x_{ob2}(k) + (I - \mathbf{\Psi_{2k}}) x_{n2}(k) \end{pmatrix} \tag{32}$$

by assuming the observers track the system states accurately, (31) can be written as:

$$\begin{pmatrix} x_{on}(k+1) \\ x_{n1}(k+1) \\ x_{n2}(k+1) \end{pmatrix} = e^{\Omega\Upsilon} \bar{\mathbf{\Psi}}(\mathbf{k}) \begin{pmatrix} x_{on}(k) \\ x_{n1}(k) \\ x_{n2}(k) \end{pmatrix} \tag{33}$$

where,

$$\hat{\mathbf{\Psi}}(\mathbf{k}) = \begin{pmatrix} I & \mathbf{0} & \mathbf{0} \\ \mathbf{\Psi_{1k}} & (I - \mathbf{\Psi_{1k}}) & \mathbf{0} \\ \mathbf{\Psi_{2k}} & \mathbf{0} & (I - \mathbf{\Psi_{2k}}) \end{pmatrix} \tag{34}$$

Let,

$$A_d = e^{\Omega\Upsilon} \hat{\mathbf{\Psi}}(\mathbf{k}) \tag{35}$$

Then (33) becomes:

$$\begin{pmatrix} x_{on}(k+1) \\ x_{n1}(k+1) \\ x_{n2}(k+1) \end{pmatrix} = A_d \begin{pmatrix} x_{on}(k) \\ x_{n1}(k) \\ x_{n2}(k) \end{pmatrix} \tag{36}$$

The existence of $\mathbf{\Psi_{1k}}$ and $\mathbf{\Psi_{2k}}$ in (36) makes the system under MIMO-ORC architecture a jump linear system (JLS) [23]. In our study, $\mathbf{\Psi_{1k}}$ or $\mathbf{\Psi_{2k}}$ can be either I or 0. Therefore, the JLS in (36) assumes four switching modes, which results in four different matrices for A_d ($= A_d(q)$ for $q = 1, .., 4$).
The JLS given in (36) is mean square stable if and only if the following holds [24]:

$$\boxed{\rho\left(\left(\mathrm{W}^T \otimes I\right) diag\left(A_d(q) \otimes A_d(q)\right)\right) < 1} \tag{37}$$

where, $\otimes$ denotes the Kronecker product, $\rho(M)$ denotes the spectral radius of M (i.e., the largest absolute value of the eigenvalues of M), $diag\left(A_d(q) \otimes A_d(q)\right)$ denotes the block diagonal matrix formed by using the matrices $A_d(q) \otimes A_d(q)$ for $q = 1, .., 4$, W denotes the state transition probability matrix of the Markov chain governing the mode switches of the system, and the dimension of the identity matrix I is determined by the sizes of A_d and W.
It can be noted from (37) that the stability of the JLS described in (36) depends on (a) the controller gain, (b) the accuracy of the 'reduced copy,' (c) sampling time Υ, and (d) the state transition probability matrix W. The following section describes the state transition probability matrix.

A. State Transition Probability Matrix (W)

As mentioned earlier, in this study, independent stochastic dropout is considered in the communication channels. Let us represent the Markov chain governing the mode switches of the system by $\{\omega_q\}$ for $q = 1, .., 4$ and the elements of W by $p_{i,j}$, which is defined by:

$$p_{i,j} = \boldsymbol{P}\left\{\omega_{q+1} = j | \omega_q = i\right\} \tag{38}$$

The four switching modes of the system are:

$$\begin{aligned}\{\omega\} = \{&\left(\mathbf{\Psi_{1k}} = I, \mathbf{\Psi_{2k}} = I\right), \left(\mathbf{\Psi_{1k}} = I, \mathbf{\Psi_{2k}} = 0\right), \\ &\left(\mathbf{\Psi_{1k}} = 0, \mathbf{\Psi_{2k}} = I\right), \left(\mathbf{\Psi_{1k}} = 0, \mathbf{\Psi_{2k}} = 0\right)\}\end{aligned} \tag{39}$$

These modes have an initial state probability distribution $\Pi_0 = [\mu_1\mu_2,\ \mu_1(1-\mu_2),\ (1-\mu_1)\mu_2,\ (1-\mu_1)(1-\mu_2)]^T$, respectively. In our study, based-on the generated stochastic independent binary data vectors $\mathbf{\Psi_{1k}}$ and $\mathbf{\Psi_{2k}}$, the matrix W is calculated. A code was developed to count the modes and the mode switches in a binary vector, then the probabilities were calculated accordingly. For example for a 75% data dropout rate in the communication channels W can be written as:

$$\mathrm{W} = \begin{bmatrix} 0.125 & 0.125 & 0.375 & 0.375 \\ 0.059 & 0.294 & 0.176 & 0.471 \\ 0.173 & 0.103 & 0.241 & 0.483 \\ 0.022 & 0.178 & 0.356 & 0.444 \end{bmatrix} \tag{40}$$

B. Dimensionality Issue for Power System Application

It is almost impractical to test the condition in (37) for a large power system model. Due to the Kronecker products in (37), the computational burden of the analysis increases with the order of A_d along with the number of switching modes of the system. Let us assume that the size of A_d is N. Then:

$$\mathrm{W}^T \otimes I = \begin{bmatrix} W^T & \mathbf{0} & \mathbf{0} & \mathbf{0} \\ \mathbf{0} & W^T & \mathbf{0} & \mathbf{0} \\ & & & \\ \mathbf{0} & \mathbf{0} & \ddots & \mathbf{0} \\ \mathbf{0} & \mathbf{0} & \mathbf{0} & W^T \end{bmatrix}_{4N^2 \times 4N^2} \tag{41}$$

and:

$$diag\left(A_d(q) \otimes A_d(q)\right) = \begin{bmatrix} A_d(1) \otimes A_d(1) & \mathbf{0} & \mathbf{0} \\ & & \\ \mathbf{0} & \ddots & \mathbf{0} \\ \mathbf{0} & \mathbf{0} & A_d(4) \otimes A_d(4) \end{bmatrix}_{4N^2 \times 4N^2} \tag{42}$$

For example, if we consider a plant representing a $15^{th}-$order model, it requires calculation of the eigenvalues of a 8100-order matrix. To reduce this computational burden, in our analysis, the reduced-order model is considered as the plant to check (37) and then the result is validated on the nonlinear

TABLE I
INTER-AREA MODES OF THE SYSTEM WITHOUT POD, WITH MIMO-ORC, AND WITH SISO-ORC

Case	No POD		MIMO-ORC		SISO-ORC	
Mode	T_s, s	f, Hz	T_s, s	f, Hz	T_s, s	f, Hz
#1	69.4	0.42	10.7	0.41	10.6	0.42
#2	28.3	0.51	14.7	0.52	14.5	0.52
#3	22.5	0.62	7.60	0.62	7.60	0.62

TABLE II
SELECTED PAIRS OF FEEDBACK SIGNALS AND CONTROL INPUT FOR DFIG PODS

Loop No.	POD	Feedback, $y_m(t)$	Control Input, $u(t)$
Loop 1	at G_9	P_{17-13}	i_{rd-mod}
Loop 2	at G_{15}	P_{18-16}	i_{rq-mod}

model using time-domain simulations.
Note that the sampling period also plays a major role in the stability of MIMO-ORC architecture. Another deciding factor for the selection of sampling period is that it should be adequate to retain the identity of the critical modes in the feedback signal. In this paper, the sampling period of PMUs and the data transmission are assumed to be 0.02 s and 0.1 s, respectively.

V. WIDE-AREA DAMPING CONTROLLER DESIGN

After inclusion of wind farms at bus-9 and bus-15, the linearized test system has three inter-area modes with frequencies (f) in the range of 0.4 - 0.7 Hz, see Table I. Poor settling times (T_s) for these modes show the need of POD at G9 and G15. Table II summarizes the control loops considered in this study where the feedback and the control input are selected based on observability and controllability of the inter-area modes, respectively. The objective of the controller is to damp these inter-area modes. The following sections highlight the controller design for MIMO-ORC and SISO-ORC.

A. MIMO-ORC Design with Simultaneous Approach

In this case, the controllers and the observers for both the loops (Loop 1 and Loop 2, see Table II) are designed simultaneously. The linearized system has three poorly damped inter-area modes and the objective of the controller is to damp these inter-area modes. A Linear Quadratic Regulator (LQR)-based controller with Luenberger type observer is designed to minimize the control effort while making sure the closed-loop system is stable with reasonable settling time for these inter-area modes. In this case, a 15^{th}-order reduced MIMO model of the original system is used as the 'reduced copy'. Table I summarizes the closed loop poles for the case of MIMO-ORC where a settling time of less than 15.0 s is achieved for all the

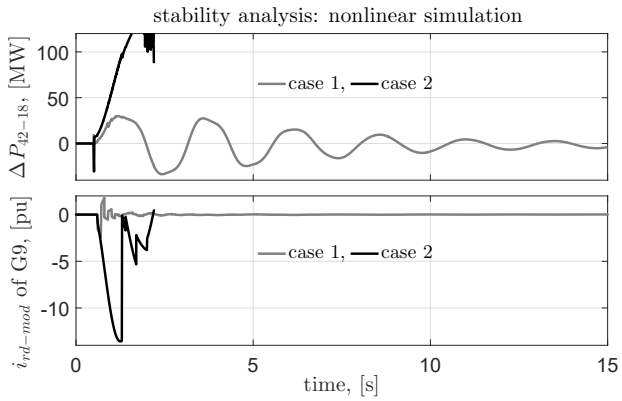

Fig. 4. Nonlinear time-domain simulation to validate the findings of the MIMO-ORC stability analysis framework.

modes. The controller gain is as follows:

$$K = \left[\begin{array}{c} 0.21, -0.07, 1.23, 1.92, -0.46, 0.24, 0.94, -0.17, \\ -0.48, 0.24, 0.34, 0.26, -0.32, 0.02, 0.17, -1.13, \\ 1.02, -0.04, -0.58, 0.19, -1.16, -1.29, -0.22 \\ 0.10, -0.26, -0.66, 0.91, 4.64, -1.29, 1.17, 14.4 \end{array}\right] \quad (43)$$

B. SISO-ORC Design with Sequential Approach

As mentioned in Section V-A an LQR-based controller is designed here as well. The SISO controller for each wind farm was designed using a sequential approach mentioned in [19]. The sequence is as follows.

- First the controller for Loop 1, see Table II, is designed considering corresponding input-output pairs to damp the selected modes (mode #1 and #3). In this case, the reduced model of the original nominal system is used for the 'reduced copy.'
- Then the closed-loop system with the controller designed for Loop 1 is considered as the plant for the Loop 2. In this case, the controller is designed to damp mode #2. For the 'reduced copy,' the reduced-model of the closed-loop system with the controller for Loop 1 is used.

To have a fair comparison between the performance of MIMO-ORC and SISO-ORC, the controller for SISO-ORC is designed in such a way that the inter-area modes of the closed-loop system will have the same settling times as of MIMO-ORC, which are highlighted in Table I. Also, the SISO 'reduced copy' considers a 15^{th}-order reduced model. The controller gains for SISO-ORC are as follows:

$$\begin{aligned} \hat{K}_1 &= [0.05,\ 0.02,\ \ 1.64, 1.97, -0.02,\ \ 0.41,\ 0.23, \\ &\quad 0.01, 0.04, -0.05,\ \ 0.12,\ 0.08, -0.27,\ \ 0.63, 0.04] \\ \hat{K}_2 &= [0.04, 0.12, -0.36, 0.57, -0.17, -0.10, -0.07, \\ &\quad 0.01, 0.03, 0.03, -0.10, 0.14, -0.10, -0.01, -0.01] \end{aligned} \quad (44)$$

The reduced-order models for both MIMO-ORC (MIMO model) and SISO-ORC (SISO model) architectures are obtained by applying the Schur Balanced Truncation method [25]. The reduced-order models are derived while retaining the identity of the inter-area modes and poorly-damped modes of the system.

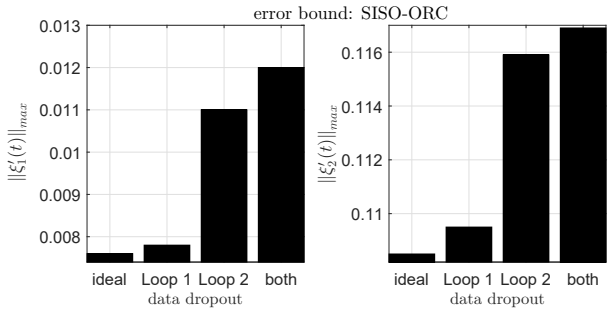

Fig. 5. Maximum error norm of state trajectories in the inter-sample interval of nominal reduced-order system for SISO-ORC from linear simulation following simultaneous pulse disturbances in both the inputs (R=25%).

The following section provides the simulation results in Matlab/Simulink platform.

VI. Simulation Results and Discussion

A. Stability Analysis of MIMO-ORC

To examine the effectiveness of the proposed stability analysis framework of MIMO-ORC, two test cases are chosen (case 1 and case 2). A 15^{th}-order linearized model of the original system is used as the plant. Independent communication models are assumed for the loops with a data receiving rate of 25% and the corresponding W given in (40) is used for the analysis. For both the cases, the condition in (37) is evaluated and the spectral radius ρ is calculated. The values for case 1 and case 2 are $\rho = 0.96$ and $\rho = 1.80$, respectively. Therefore, it can be concluded that case 1 is stable and case 2 is unstable. The findings of this analysis was validated using nonlinear time-domain simulations, which are shown in Fig. 4.

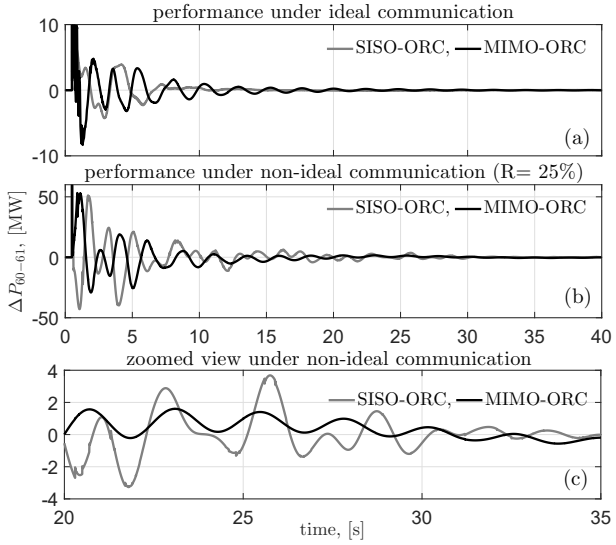

Fig. 6. Performance of SISO-ORC versus MIMO-ORC for a self-clearing fault near bus 60, see Fig. 2, under (a) ideal (R=100%) and (b) non-ideal (R=25%) communication. (c) Zoomed view between t = 20.0s - 35.0s for the case of non-ideal communication.

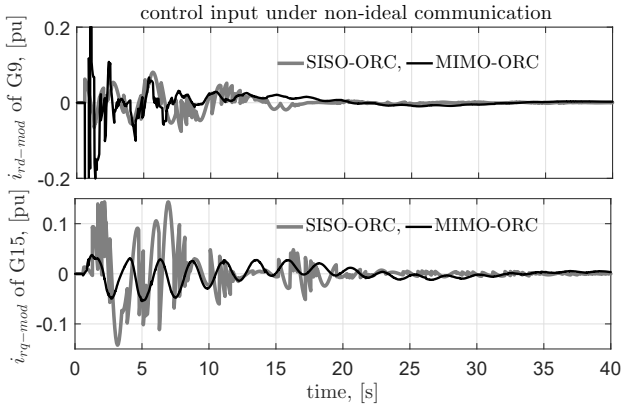

Fig. 7. Comparison of control input signals of SISO-ORC versus MIMO-ORC for a self-clearing fault near bus 60, see Fig. 2, under non-ideal (R=25%) communication.

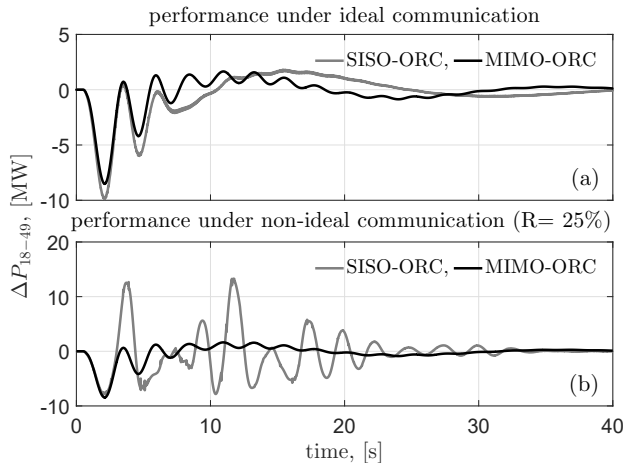

Fig. 8. Performance of SISO-ORC versus MIMO-ORC following a pulse change in the wind speed (V_w) at the wind farm G15, under (a) ideal (R=100%) and (b) non-ideal (R=25%) communication.

B. MIMO-ORC vs SISO-ORC: Performance Evaluation

The performance of the proposed MIMO-ORC was compared with the SISO-ORC using linear and nonlinear simulation under different disturbances in the power system along with different data receiving rates in the communication links. For all the cases, independent stochastic dropout with R=25% is considered in the two communication channels, which are represented using Gilbert-Elliott model.

To validate the claims of Remark I and Remark II, linear time-domain simulations are carried out using a 15^{th}-order model of the nominal system, which neglects the observer dynamics. It was observed that the MIMO-ORC produces zero inter-sample error. On the other hand, the SISO-ORC results in non-zero error. Figure 5 shows the maximum inter-sample error norm calculated for the SISO-ORC case. It can be observed from Fig. 5 that the maximum error norm of each loop increases with non-ideality of the communication links due to the cyber-physical 'self-coupling' and 'cross-coupling'.

To compare the performance of the MIMO-ORC with the SISO-ORC under nominal operating condition of the physical layer, a three-phase self-clearing fault near bus 60, see Fig. 2,

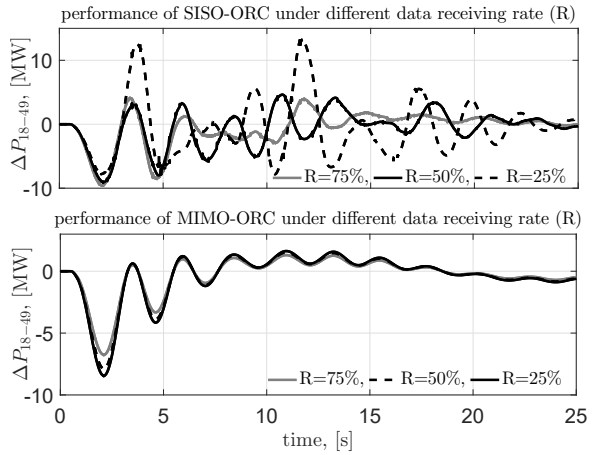

Fig. 9. Performance of SISO-ORC versus MIMO-ORC following a pulse change in the wind speed (V_w) at the wind farm G15, under different data receiving rates.

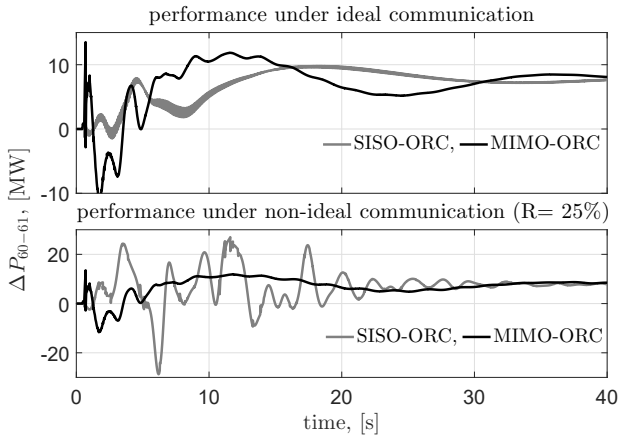

Fig. 10. Performance of SISO-ORC versus MIMO-ORC after a 100 MW step increase in total system load, under ideal (R=100%) and non-ideal (R=25%) communication.

is considered. For the non-ideal communication case, a 25% data receiving rate in both the communication links are assumed. Figures 6 and 7 show the dynamic performance of the nonlinear system and control input signals, respectively. The observations are:

- Under ideal communication, both SISO-ORC and MIMO-ORC give satisfactory damping performance (Fig. 6.a).
- Low data receiving rate deteriorates the performance of both MIMO-ORC and SISO-ORC. However, the deterioration is less for MIMO-ORC (Fig. 6.b, and Fig. 6.c).
- Under non-ideal communication, the difference between states of the reduced copies in MIMO-ORC and the states estimated by the observer is smaller compared to SISO-ORC. This produces larger jumps in the control input $u(t)$ during re-setting (Fig. 7).
- DFIG turbine-generator's torsional stress is much less in the case of MIMO-ORC since it captures the system dynamics closely during data dropouts, which produces less jumps in the control inputs i_{rd-mod} or i_{rq-mod}.

To study the effect of wind speed variation on the performance of MIMO-ORC, a pulse change in the wind speed is considered. Figure 8 shows the dynamic performance of the system following a pulse change in the wind speed at the wind farm G15. It can be observed from Fig. 8 that under ideal communication both MIMO-ORC and SISO-ORC produces almost same damping performance. Figure 9 compares the performance of MIMO-ORC versus SISO-ORC under different data receiving rates, which reveals that under non-ideal communication MIMO-ORC produces better damping performance compared to that of SISO-ORC.

To study the effect of the operating condition on the MIMO-ORC performance, dynamic performance of the system following a 100 MW step increase in total system load is compared against SISO-ORC, see Fig. 10 and Fig. 11, which reveal:

- Under ideal communication, satisfactory damping performance can be observed for both architectures.
- Under low data reeving rates, MIMO-ORC performance is slightly poorer than that of ideal communication scenario.
- The performance of MIMO-ORC is better than that of SISO-ORC under high data dropouts.

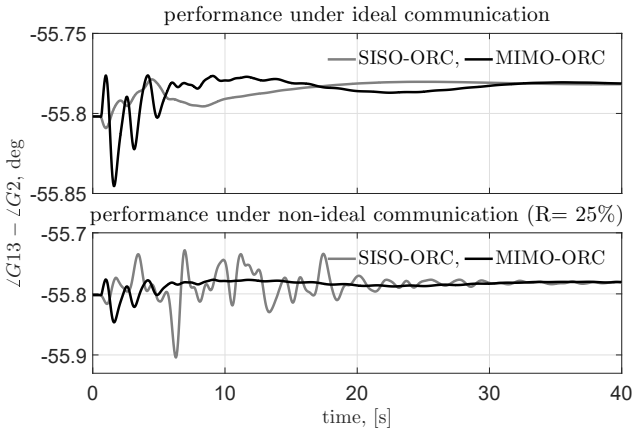

Fig. 11. Performance of SISO-ORC versus MIMO-ORC after a 100 MW step increase in total system load, under ideal (R=100%) and non-ideal (R=25%) communication.

VII. Conclusion

In this paper, a new MIMO-ORC architecture is proposed for wide-area damping control using multiple DFIG-based wind farms to deal with data packet dropout. It was shown that the proposed architecture is less sensitive to data dropout compared to its SISO-ORC counterpart. Our ongoing research is focused on the performance and stability analysis of MIMO-ORC architecture under latency along with data dropout.

Appendix

To find the Λ in (19), let, $Z = \Lambda^{-1}$. From the Lemma (9.1.3) of [22] if:

$$Z = \begin{bmatrix} Z_{11} & Z_{12} \\ Z_{21} & Z_{22} \end{bmatrix} \tag{45}$$

Then:

$$Z^{-1} = \begin{bmatrix} P_1^{-1} & -Z_{11}^{-1} Z_{12} P_2^{-1} \\ -P_2^{-1} Z_{21} Z_{11}^{-1} & P_2^{-1} \end{bmatrix} \tag{46}$$

where:

$$P_1 = Z_{11} - Z_{12}Z_{22}^{-1}Z_{21}, \quad P_2 = Z_{22} - Z_{21}Z_{11}^{-1}Z_{12} \tag{47}$$

In our case:

$$\begin{aligned} Z_{11} &= \begin{bmatrix} sI - A_{on} & B_{on1}K_1 \\ \mathbf{0} & sI - (A_n - B_nK) \end{bmatrix}, \\ Z_{12}^T &= \begin{bmatrix} B_{on2}{K_2}^T & \mathbf{0} \end{bmatrix}, Z_{21} = \begin{bmatrix} \mathbf{0} & \mathbf{0} \end{bmatrix}, \\ Z_{22} &= sI - (A_n - B_nK) \end{aligned} \tag{48}$$

REFERENCES

[1] X. Y. Bian, Y. Geng, K. L. Lo, Y. Fu, and Q. B. Zhou, "Coordination of psss and svc damping controller to improve probabilistic small-signal stability of power system with wind farm integration," *IEEE Trans. on Power Systems*, vol. 31, no. 3, pp. 2371–2382, May 2016.

[2] L. Zacharia, L. Hadjidemetriou, and E. Kyriakides, "Integration of renewables into the wide area control scheme for damping power oscillations," *IEEE Trans. on Power Systems*, vol. 33, no. 5, pp. 5778–5786, 2018.

[3] M. Mokhtari and F. Aminifar, "Toward wide-area oscillation control through doubly-fed induction generator wind farms," *IEEE Trans.on Power Systems*, vol. 29, pp. 2985–2992, 2014.

[4] T. Surinkaew and I. Ngamroo, "Hierarchical co-ordinated wide area and local controls of DFIG wind turbine and PSS for robust power oscillation damping," *IEEE Trans. on Sustainable Energy*, vol. 7, pp. 1–13, 2016.

[5] A. E. Leon and J. A. Solsona, "Power oscillation damping improvement by adding multiple wind farms to wide-area coordinating controls," *IEEE Trans. on Power Systems*, vol. 29, pp. 1356–1364, 2014.

[6] L. Lamarre, "At home with communications," *EPRI Journal*, pp. 7–15, January/February 1997.

[7] G. N. Ericsson, "Communication requirements - basis for investment in a utility wide-area network," *IEEE Trans. on Power Delivery*, vol. 19, no. 1, pp. 92–95, 2004.

[8] Radio Subcommittee of IEEE Power System Communications Committee, "Analog/digital microwave considerations for electric/gas utilities," *IEEE Trans. on Power Delivery*, vol. 8, no. 3, pp. 798–815, 1993.

[9] D. Radford, "Spread spectrum data leap through ac power wiring," *IEEE Spectrum*, vol. 33, no. 11, pp. 48–53, 1996.

[10] D. Schneider, "Is this the moment for broadband over power lines?" *IEEE Spectrum*, vol. 46, no. 7, pp. 17–17, 2009.

[11] L. A. Montestruque and P. J. Antsaklis, "On the model-based control of networked systems," *Automatica*, vol. 39, no. 10, pp. 1837–1843, 2003.

[12] P. V. Zhivoglyadov and R. H. Middleton, "Networked control design for linear systems," *Automatica*, vol. 39, no. 4, pp. 743–750, 2003.

[13] L. A. Montestruque and P. Antsaklis, "Stability of model-based networked control systems with time-varying transmission times," *IEEE Trans. on Automatic Control*, vol. 49, no. 9, pp. 1562–1572, 2004.

[14] E. Garcia and P. J. Antsaklis, "Model-based control of continuous-time systems with limited intermittent feedback," in *21st Mediterranean Conference on Control and Automation*, June 2013.

[15] N. R. Chaudhuri, D. Chakraborty, and B. Chaudhuri, "An architecture for FACTS controllers to deal with bandwidth-constrained communication," *IEEE Trans. on Power Delivery*, vol. 26, no. 1, pp. 188–196, 2011.

[16] A. Singh, R. Singh, and B. Pal, "Stability Analysis of Networked Control in Smart Grids," *IEEE Trans. on Smart Grid*, vol. 6, pp. 381–390, 2015.

[17] A. Yogarathinam and N. R. Chaudhuri, "Wide-area damping control using multiple DFIG-based wind farms under stochastic data packet dropouts," *IEEE Trans. on Smart Grid*, vol. 9, no. 4, pp. 3383–3393, July 2018.

[18] ——, "Wide-area damping control using reduced copy under intermittent observation: A novel performance measure," *IEEE Trans. on Control Systems Technology*, vol. 27, no. 1, pp. 434–442, Jan 2019.

[19] B. Pal and B. Chaudhuri, *Robust control in power systems*, ser. Power electronics and power systems. New York: Springer, 2005.

[20] R. Pena, J. C. Clare, and G. M. Asher, "Doubly fed induction generator using back-to-back PWM converters and its application to variable-speed wind-energy generation," *IEE Proceedings on Electric Power Applications*, vol. 143, no. 3, pp. 231–241, 1996.

[21] A. Yogarathinam, J. Kaur, and N. R. Chaudhuri, "Impact of inertia and effective short circuit ratio on control of frequency in weak grids interfacing LCC-HVDC and DFIG-based wind farms," *IEEE Trans. on Power Delivery*, vol. 32, pp. 2040–2051, 2016.

[22] K. B. Petersen and M. S. Pedersen, *The Matrix Cookbook*. Technical University of Denmark, 2012.

[23] Y. Fang and K. A. Loparo, "Stochastic stability of jump linear systems," *IEEE Trans. on Automatic Control*, vol. 47, no. 7, pp. 1204–1208, Jul 2002.

[24] V. Gupta, R. M. Murray, L. Shi, and B. Sinopoli, *Networked sensing, estimation and control systems*. Tech. Rep. Dept. Control Dyn. Syst, California Inst. Technol., Pasadena, CA, USA, 2009.

[25] M. G. Safonov and R. Y. Chiang, "A schur method for balanced-truncation model reduction," *IEEE Trans. on Automatic Control*, vol. 34, no. 7, pp. 729–733, July 1989.

Amirthagunaraj 'Raj' Yogarathinam (S'12) received the B.E. degree in electrical and electronic engineering from the University of Peradeniya, Sri Lanka, in 2013. He is currently pursuing the Ph.D. degree with the Pennsylvania State University, PA, USA. He was a Researcher and an Instructor with the Department of Electrical and Electronic Engineering, University of Peradeniya, from 2013 to 2014. He has also worked as a research intern at Argonne National Laboratory during summer 2018. His research interests include power system dynamics and control, MTDC, Hybrid-MTDC, wind power integration to the modern grid, wide-area monitoring and control, application of power electronics in power systems, online system identification, and smart grid.

Nilanjan Ray Chaudhuri (S'08-M'09-SM'16) received his Ph.D. degree from Imperial College London, London, UK in 2011 in Power Systems. From 2005-2007, he worked in General Electric (GE) John F. Welch Technology Center. He came back to GE and worked in GE Global Research Center, NY, USA as a Lead Engineer during 2011-2014. Presently, he is an Assistant Professor with the School of Electrical Engineering and Computer Science at Penn State, University Park, PA. He was an Assistant Professor with North Dakota State University, Fargo, ND, USA during 2014-2016. He is a member of the *IEEE* and *IEEE PES*. Dr. Ray Chaudhuri is the lead author of the book *Multi-terminal Direct Current Grids: Modeling, Analysis, and Control* (Wiley/IEEE Press, 2014), and an Associate Editor of the IEEE TRANSACTIONS ON POWER DELIVERY. Dr. Ray Chaudhuri is the recipient of the National Science Foundation Early Faculty CAREER Award in 2016.